Journal of
Applied Crystallography

ISSN 0021-8898

Received 16 August 2006
Accepted 22 December 2006

Pore lattice deformation in ordered mesoporous silica studied by *in situ* small-angle X-ray diffraction

Gerald A. Zickler,[a] Susanne Jähnert,[b] Sérgio S. Funari,[c] Gerhard H. Findenegg[b] and Oskar Paris[a]*

[a]Department of Biomaterials, Max Planck Institute of Colloids and Interfaces, Research Campus Golm, D-14424 Potsdam, Germany, [b]Stranski Laboratory of Physical and Theoretical Chemistry, Technical University Berlin, Straße des 17. Juni 135, D-10623 Berlin, Germany, and [c]Hamburger Synchrotronstrahlungslabor (HASYLAB), Deutsches Elektronen-Synchrotron (DESY), Notkestraße 85, D-22603 Hamburg, Germany. Correspondence e-mail: oskar.paris@mpikg.mpg.de

Sorption and capillary condensation of an organic fluid in ordered mesoporous silica were studied by *in situ* small-angle X-ray diffraction using synchrotron radiation. The sorption isotherm was calculated from the sample transmission data. The diffraction peaks resulting from the periodic hexagonal arrangement of the pores show characteristic changes of intensity, position and width, and a pronounced hysteresis of these parameters in the capillary condensation/evaporation regime was observed. The change of the peak positions with gas pressure is related to pore lattice deformations due to capillary stresses occurring at the gas–liquid phase transition.

1. Introduction

During the last decade, much progress has been made in the design, synthesis and characterization of inorganic mesoporous materials with pores of long-range order, such as MCM-41 (Kresge *et al.*, 1992) or SBA-15 (Zhao *et al.*, 1998). These novel materials are of importance for a wide range of applications, such as separation processes, heterogeneous catalysis and gas storage. They also represent ideal model systems for studying adsorption and capillary condensation of fluids in confined geometries (Evans, 1990; Gelb *et al.*, 1999; Christenson, 2001). The filling of nanometre-sized pores usually proceeds *via* the formation of an adsorbed film, which grows in thickness with increasing vapour pressure until a sharp increase of the adsorbed amount occurs due to capillary condensation of the vapour. Capillary condensation represents a first-order phase transition and exhibits a pronounced hysteresis with respect to adsorption and desorption.

While there is an ever growing interest in the phase behaviour of fluids and fluid mixtures in the confined environment of mesopores (Gelb *et al.*, 1999; Alba-Simionesco *et al.*, 2006), less attention has been paid to the deformation of the solid pore walls due to interaction with the adsorbing liquid. However, mechanical stability of mesoporous materials is of great relevance for practical purposes. Besides external stresses, which can occur during synthesis, processing and application of porous materials (Gusev *et al.*, 1996; Hartmann & Bischof, 1999, Hartmann & Vinu, 2002; Cassiers *et al.*, 2002; Desplantier-Giscard *et al.*, 2003), pressure differences between the liquid and gas phases during sorption of fluids may result in pore wall deformations. This is particularly true for capillary condensation or capillary evaporation, with the maximum capillary stress occurring at the vapour pressure at which liquid bridges with highly curved menisci form or disappear in the pore. Prominent examples of this phenomenon are the deformation of narrow silicon nanostructures upon cleaning with water and successive drying (Namatsu *et al.*, 1995) or the drying of gels (Scherer, 1992). The deformation of the extremely compliant pore walls in gels may considerably influence the details of the measured adsorption isotherm. This affects the calculations of the pore size distribution (Reichenauer, 2004), allowing an estimation of the compression modulus of the material under specific circumstances (Reichenauer & Scherer, 2000; Reichenauer, 2004). The capillary stresses of fluids with low surface tension such as nitrogen are typically in the range of a few MPa for not too small pore sizes, which has been considered to be negligible for mesoporous materials so far (Reichenauer, 2004). However, in many practical cases of fluid sorption much higher pressures can be expected, due to high surface tension of the fluid (*e.g.* H_2O) and very narrow pores with radii ≤ 1 nm.

Dolino *et al.* (1996) were the first to study the deformation of pore walls of porous Si as a function of pentane vapour pressure by applying *in situ* X-ray diffraction. Whereas pore wall deformations are difficult to measure in the case of amorphous materials (SiO_2), deformations of the pore lattice of ordered materials such as MCM-41 and SBA-15 can be investigated by small-angle diffraction. So far, only a few *in situ* sorption experiments of fluids in mesoporous materials have been conducted by X-ray (Mitropoulos *et al.*, 1995; Albouy & Ayral, 2002; Hofmann *et al.*, 2005; Zickler *et al.*, 2006) and neutron diffraction (Smarsly *et al.*, 2001; Hoinkis, 2004; Melnichenko *et al.*, 2006). None of these were focused specifically on the effect of lattice deformations, although a slight change of the pore lattice parameter upon capillary condensation has already been noted by Albouy & Ayral (2002).

In the present work, *in situ* small-angle X-ray diffraction was used to study the pore wall deformation of mesoporous silica SBA-15 due to capillary condensation and capillary evaporation of an organic fluid (perfluoropentane, C_5F_{12}). The experiments were performed using a custom-made sorption cell at a high-brilliance synchrotron radiation source, allowing a detailed analysis of the small-angle diffraction profiles as a function of vapour pressure.

2. Experimental

SBA-15 silica was synthesized according to the description of Zhao *et al.* (1998) using the technical-grade triblock copolymer Pluronic 123 as the structure-directing template in aqueous H_2SO_4 solution, and tetraethyl orthosilicate as the silicate source. The synthesis, hydrothermal treatment and calcination of the material followed a similar protocol to that given by Hofmann *et al.* (2005).

For *in situ* small-angle synchrotron X-ray diffraction in conjunction with sorption, a special apparatus was designed (Fig. 1). The specimen chamber was made of aluminium and the cell windows were equipped with Kapton foils. SBA-15 powder was carefully pressed to a stable pellet of 0.3 mm thickness and 3 mm diameter. The sorption cell was temperature-controlled by Peltier devices and had an internal flow system, which was connected *via* pipes to the liquid adsorbent in a reservoir. The gas was supplied to the sample in the sorption chamber through a gas dosing valve and the vapour pressure was measured with a Baratron pressure gauge (MKS Instruments). Before starting a sorption experiment, the specimen was evacuated at a temperature of 353 K and a pressure below 10^{-5} mbar for one hour. For sorption experiments, the cell was thermostated at 290 K (to be the coldest point in the system), and the reservoir stayed at ambient temperature of 294 K. The liquid adsorbent (C_5F_{12}, ABCR Chemicals) was used as received. The sorption cell was controlled remotely by a custom-written software program based on Hewlett-Packard *HP VEE*, which allowed continuous adsorption and desorption scans.

Small-angle X-ray diffraction measurements were performed at the beamline A2 (Elsner *et al.*, 1985) at the Hamburger Synchrotronstrahlungslabor (HASYLAB), Deutsches Elektronen-Synchrotron (DESY) in Hamburg, Germany. The synchrotron radiation was monochromated by a germanium 111 crystal to an energy E of 8.27 keV ($\Delta E/E = 10^{-3}$), focused by a single mirror, and the cross section of the beam was defined by aperture slits to 2 mm (horizontally) × 0.5 mm (vertically) at the sample position. A CCD X-ray area detector (MarCCD 165, Mar USA) with a resolution of 2048 × 2048 pixels (pixel size: 79 × 79 μm^2) was used to detect the scattered photons. The sample-to-detector distance was determined by calibrating with a standard reference sample of silver behenate. The X-ray diffraction patterns covered a range of the scattering vector q of 0.3 nm^{-1} < q < 2.4 nm^{-1}. The length of the scattering vector is given by $q = (4\pi/\lambda)\sin\theta$, with 2θ being the scattering angle and λ the wavelength. Vacuum flight tubes were inserted between the sample and the detector in order to avoid air scattering. The transmission of the sample at each sorption state was determined using an ionization chamber before the adsorption cell to monitor the primary synchrotron X-ray flux and a photodiode mounted in the beamstop to measure the transmitted photons.

A typical exposure time of 60 s yielded a scattering pattern with excellent counting statistics. The scattering patterns were corrected for background scattering, electronic noise, transmission and polarization using the data reduction program *Fit2D* (Hammersley *et al.*, 1996). All specimens showed isotropic scattering patterns (powder rings), which were azimuthally averaged in vertical sectors of 40° for equal radial distances from the central beam.

3. Results

Seven diffraction peaks were resolved in the small-angle X-ray diffraction profiles of SBA-15, corresponding to the 10, 11, 20, 21, 30, 22 and 31 diffraction peaks of the two-dimensional hexagonal lattice (Fig. 2). The intensity of the individual diffraction peaks changed with the variation of the vapour pressure, according to the changes of the form factor of the silica/adsorbed film/pore system (Zickler *et al.*, 2006).

After reaching the capillary condensation regime, a strong decrease of the peak intensities was observed. The effects were fully reversible, *i.e.* after desorption the initial state was reached again. In addition to the diffraction peaks, a diffuse small-angle scattering signal was observed, which also changed with varying vapour pressure. This signal may be related to weakly ordered heterogeneities such as micropores or pore wall roughness, which are also affected (*e.g.* filled) during sorption. For separation of the diffraction peak from the diffuse scattering, each peak was fitted separately by a custom-written software program, using a pseudo-Voigt function and a first-order polynomial as baseline. Peak positions, full widths at half peak maximum (FWHM) and peak areas were free fit parameters and no constraints were set.

It is an important aspect of the experiments that the corresponding sorption isotherm, expressed as adsorbed mass *versus* relative pressure p/p_0, can be obtained from measuring the transmission of the

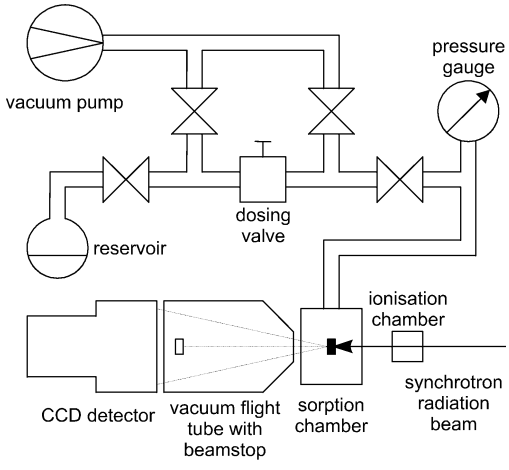

Figure 1
Schematic representation of the setup of the *in situ* apparatus at beamline A2 at the Hamburger Synchrotronstrahlungslabor (HASYLAB), Deutsches Elektronen-Synchrotron (DESY) in Hamburg, Germany.

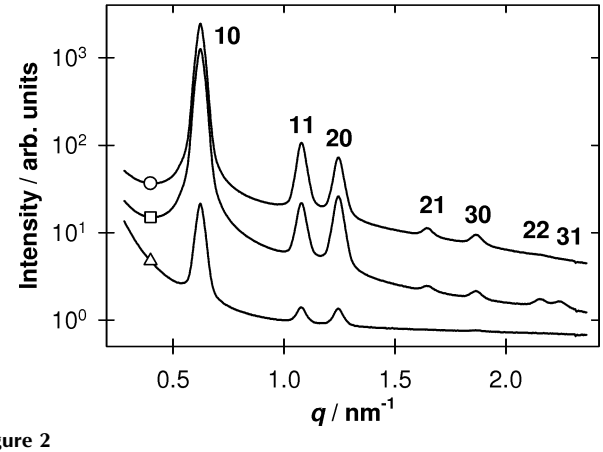

Figure 2
A series of small-angle X-ray diffraction profiles (scattering intensity *versus* length of scattering vector) during adsorption of C_5F_{12} in SBA-15 for $p/p_0 = 0$ (circle), 0.28 (square) and 0.87 (triangle). The curves are shifted vertically by a factor of three with respect to each other for the sake of clarity. The profile at $p/p_0 = 0.87$ represents a state above capillary condensation where the intensity is lowered due to partial contrast matching of the liquid C_5F_{12} with the SBA-15 matrix.

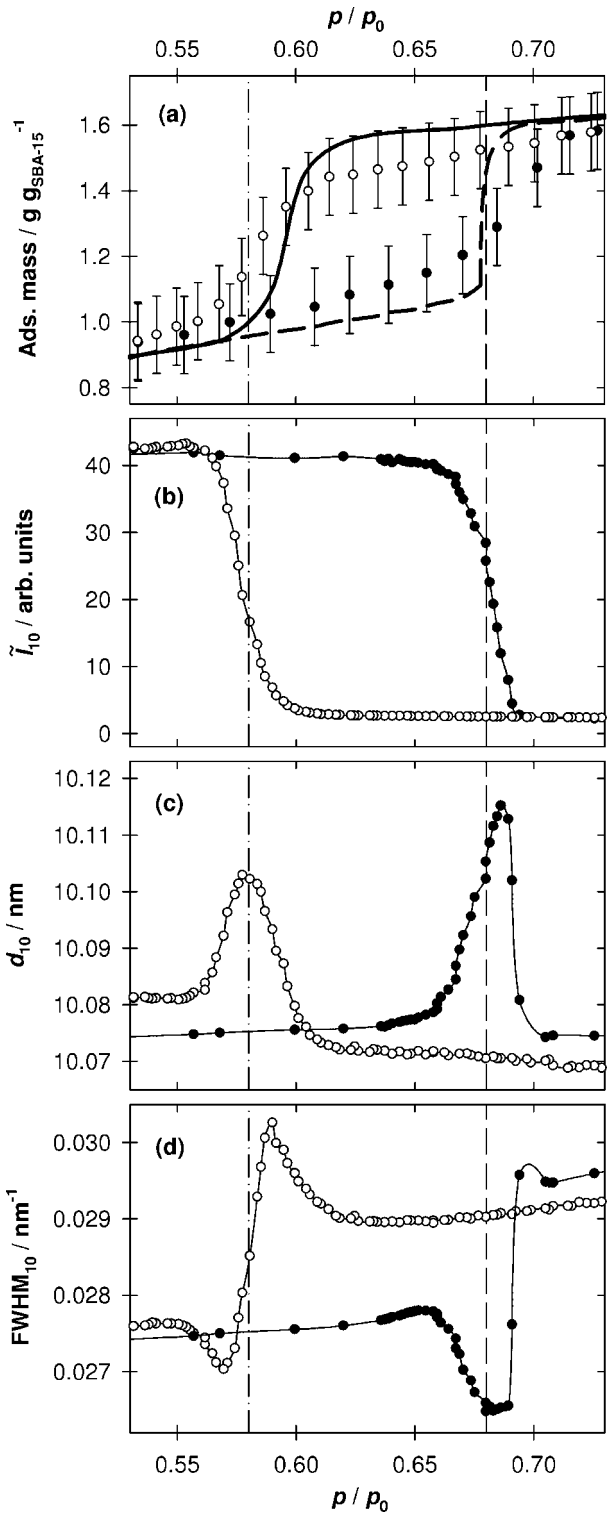

Figure 3
(*a*) Adsorption isotherm (dashed line) and desorption isotherm (solid line) of C_5F_{12} in SBA-15 (relative adsorbed mass m_F/m_M *versus* relative pressure p/p_0) measured with a microbalance and calculated from the *in situ* transmission measurements, respectively. The filled symbols denote the adsorption scan and the open symbols indicate the desorption scan. The error bars represent an estimated uncertainty of $\pm$ 3% in the determination of the specimen transmission. The pressures at capillary condensation and capillary evaporation are represented by vertical dashed lines and dash-dotted lines, respectively (Zickler *et al.*, 2006). (*b*) Integrated intensity $\tilde{I}_{10}$, (*c*) lattice spacing d_{10}, and (*d*) full width at half maximum, $FWHM_{10}$, of the 10 diffraction peak as a function of vapour pressure for adsorption and desorption scans of C_5F_{12} in SBA-15.

specimen *in situ*. The sample transmission τ is given by $\tau = \exp(-\mu D)$, with $\mu D = (\mu/\rho)_M \rho_M D_M + (\mu/\rho)_F \rho_F D_F$, where (μ/ρ) is the sample mass absorption coefficient for the chosen X-ray energy, ρ is the sample density and D is the irradiated sample thickness. The superscripts M and F correspond to the silica matrix of SBA-15 and the adsorbed fluid, respectively. The adsorbed mass m is proportional to $\rho_F D_F$ and from this a linear relationship between the relative adsorbed mass m_F/m_M and $\ln(\tau)$ is derived,

$$\frac{m_F}{m_M} = \frac{-\left[C\, m_M\, \ln(\tau) + (\mu/\rho)_M\right]}{(\mu/\rho)_F}, \qquad (1)$$

where the constants C and m_M were determined from the evacuated sample. The sorption isotherm from transmission data was calculated by adopting the values $(\mu/\rho)_M = 33.52\ cm^2\ g^{-1}$ for bulk silica and $(\mu/\rho)_F = 12.40\ cm^2\ g^{-1}$ for C_5F_{12}. Fig. 3(*a*) shows a comparison of the sorption isotherm determined with a microbalance and the calculated isotherm from *in situ* transmission measurements. The differences between the results of the two methods are most likely due to experimental uncertainties of the sample transmission measurements and to possible non-equilibration of the respective adsorption state. Nevertheless, Fig. 3(*a*) clearly demonstrates that, in principle, the sample transmission is suitable to determine sorption isotherms of fluids in porous solids.

Fig. 3(*b*) shows the integrated intensity $\tilde{I} = \int I(q_{hk})\, q^2\, dq$ of the 10 diffraction peak as a function of relative vapour pressure p/p_0 during adsorption and desorption of C_5F_{12} in SBA-15. The integrated intensities of all measured diffraction peaks (Fig. 2) show characteristic changes with pressure and a distinct hysteresis is observed between condensation and evaporation. The d-spacing of the 10 diffraction peak was calculated by $d_{10} = 2\pi/q_{10}$, with q_{10} being the peak position as seen in Fig. 3(*c*). It is obvious that capillary condensation and evaporation lead to a considerable expansion of the pore lattice at the respective pressure values. The pressure dependence of FWHM (Fig. 3*d*) exhibits a pronounced hysteresis, showing a slight peak narrowing at the onset of capillary condensation and at the end of pore evaporation, respectively. For higher pressures a considerable peak broadening (up to 10%) is observed. As can be seen in Figs. 3(*c*) and 3(*d*), there are slight differences in the absolute values for the adsorption and desorption branches. This might be due to experimental uncertainties, such as a small temperature drift, or an insufficient equilibration leading to kinetic effects. Given that the maximum peak shift is about a factor of ten smaller than the peak width, some uncertainty in the fit due to a coupling of the parameters is also possible. Nonetheless, the trends in the pressure dependence of the parameters were found in several independent measurements.

4. Discussion

In situ small-angle X-ray diffraction using high-brilliance synchrotron radiation was employed to study sorption and capillary condensation of an organic fluid in mesoporous silica. The sorption isotherm was determined from the specimen transmission, simultaneously with the diffraction patterns as a function of vapour pressure. Up to seven diffraction peaks from the two-dimensional hexagonal pore lattice of SBA-15 could be measured and analysed with high accuracy. The integrated intensities of all seven observed diffraction peaks changed systematically as function of vapour pressure over the whole pressure range. In a recent study, Zickler *et al.* (2006) analysed these characteristic changes by applying a four-density-level model for the scattering contrast of C_5F_{12} sorption in SBA-15, allowing the deter-

mination of the detailed structure of the evacuated sample and the thickness of the adsorbed film during adsorption and desorption, respectively. At pressures above capillary condensation, the mesopores were completely filled and the integrated intensities of the diffraction peaks strongly decreased, due to the fact that the adsorbed fluid nearly matched the scattering length density of the silica matrix.

As shown in the present work, not only do the integrated intensities of the individual diffraction peaks change with pore filling, but also a shift of the peak positions corresponding to a change of the pore lattice spacing is clearly observed. The effect is reversible and exhibits the well known hysteresis between adsorption and desorption. As can be seen in Fig. 3(*c*), the maximum change of the d_{10}-spacing is of the order of 0.3%. At capillary condensation, the Laplace pressure (pressure difference across the meniscus of the fluid) $\Delta p = 2\gamma/r$ can be calculated by inserting $\gamma \approx 0.01$ J m^{-2} for the surface tension of C_5F_{12} and $r \approx 3.3$ nm for the radius of the liquid-coated pore at capillary condensation (Zickler *et al.*, 2006). The total deformation of the silica matrix ε can then be estimated by assuming the mechanical behaviour of a honeycomb structure, $\varepsilon = \Delta p\ (1-2\nu)\ /\ [E\ (1-P)^3]$ (Gibson & Ashby, 1999), where P is the porosity, and ν and E are the Poisson's ratio and the elastic modulus of bulk silica, respectively. Inserting $P \approx 0.7$ (Zickler *et al.*, 2006), $E \approx 94$ GPa and $\nu \approx 0.17$, one finds a strain $\varepsilon \approx 0.16\%$. This value is about a factor of two smaller than the experimentally observed value (Fig. 3*c*), which is taken as fair agreement in view of the many assumptions. However, while the absolute value of the strain agrees well with this simple estimate, the direction of the strain (tensile) is not immediately clear. Albouy & Ayral (2002) also reported a slight pore lattice expansion upon capillary condensation of nitrogen in MCM-41, but they did not make any attempts to explain their observation. By similarity with the behaviour of gels, one would expect a contraction of the sample at capillary condensation followed by a re-expansion (Reichenauer, 2004). However, the present measurements show that exactly the opposite happens with the hexagonal pore lattice in ordered mesoporous materials. The lattice clearly expands during capillary condensation and then relaxes back to approximately the starting value, and the same occurs at the desorption branch (Fig. 3*c*). Fig. 4 shows a simple picture illustrating schematically a possible explanation. At the onset of capillary condensation, the pores of smallest diameter are filled first and induce a negative pressure on the surrounding pore wall. Between two filled pores, a tensile stress would be induced, leading eventually to a local expansion of the lattice. It is plausible that this effect increases with increasing fraction of filled pores ϕ up to the point $\phi = 0.5$ and then decreases again to reach its original value as ϕ approaches 1.

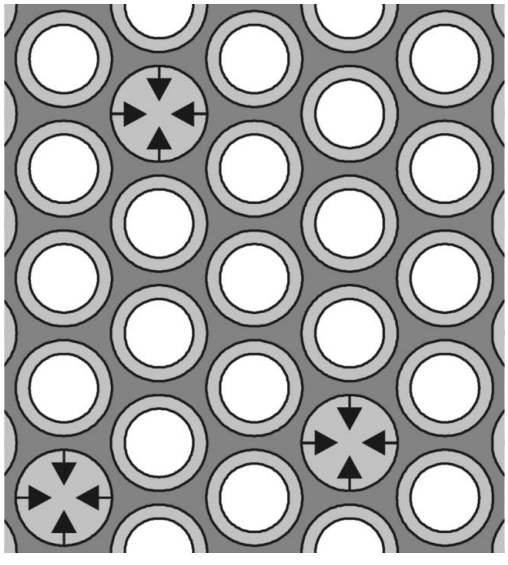

Figure 4
Schematic model of pore wall deformation due to strains of adsorption and capillary condensation of a liquid in mesoporous silica. Dark grey: solid silica matrix; light grey: adsorbed liquid film; white: unfilled core. The arrows indicate the negative stress upon capillary condensation in a pore, which causes an expansion of the lattice in the neighbourhood of the filled pores.

As can be seen in Fig. 3(*d*), there is also a change in the width of the diffraction peaks. The initial reduction of the width is somewhat unexpected and suggests that inhomogeneous lattice strains are already present in the empty sample, presumably due to a finite pore size distribution. The filling of the smallest pores at the onset of capillary condensation may release these strains, leading to an initial narrowing of the diffraction peaks. The subsequent peak broadening can have two sources: either an inhomogeneous strain distribution is established upon continuous pore filling, or domains of filled/unfilled pores lead to a peak broadening due to the finite domain size. An influence of the local pore wall deformation on the condensation behaviour of neighbouring pores could indeed lead to collective phenomena such as the formation of domains. A further possible explanation for the peak broadening is based on anisotropic deformation of the lattice. An elliptical distortion of the originally circular pores due to buckling of the pore walls along the thin-walled directions is conceivable. This effect would primarily induce a peak splitting due to the deviation from hexagonal symmetry, which besides a peak broadening would also result in a net peak shift. From our experimental data, the 11 diffraction peak shows a very similar trend to the 10 peak, suggesting isotropic deformation. However, it should be kept in mind that the 11 peak is much smaller than the 10 peak and almost disappears close to capillary condensation due to a minimum of the form factor (Zickler *et al.*, 2006). A quantification of this concept would require a detailed peak profile analysis of several diffraction peaks, preferably from measurements with better instrumental resolution. This was, however, beyond the scope of this paper.

5. Conclusion

Adsorption and desorption of an organic fluid in mesoporous silica SBA-15 were studied by *in situ* small-angle diffraction using synchrotron radiation. The sample transmission and the first seven diffraction peaks resulting from the two-dimensional hexagonal packing of the cylindrical mesopores were measured *in situ* as a function of the vapour pressure of the adsorbent. From the sample transmission data the sorption isotherm of the fluid was calculated. Integrated intensity, peak position and FWHM were evaluated by least-squares fitting of each individual diffraction peak. The parameters obtained showed characteristic changes with pressure, including pronounced hysteresis in the pressure region of capillary condensation and pore evaporation. The shift of the diffraction peaks close to capillary condensation and evaporation indicates reversible deformation of the silica matrix pore walls. A simple estimate of the expected deformation strain in honeycomb foams agrees with the experimentally observed changes of the *d*-spacing. Interestingly, the pore lattice exhibits tensile strain, which is qualitatively discussed. The detailed deformation mechanisms are not yet fully clear and need further investigation.

The authors thank E.-P. Resewitz and M. Taherkhani (Stranski Laboratory) for providing assistance with the construction and testing of the *in situ* sorption apparatus, and W. Wagermaier (Max Planck Institute) and M. Dommach (HASYLAB, DESY) for help with the synchrotron radiation experiments. Financial support from the Deutsche Forschungsgemeinschaft (SFB 448, TP B1) and from the Max Planck Society is gratefully acknowledged.

References

Alba-Simionesco, C., Coasne, B., Dosseh, G., Dudziak, G., Gubbins, K. E., Radhakrishnan, R. & Sliwinska-Bartkowiak, M. (2006). *J. Phys. Condens. Matter*, **18**, R15–R68.
Albouy, P.-A. & Ayral, A. (2002). *Chem. Mater.* **14**, 3391–3397.
Cassiers, K., Linssen, T., Mathieu, M., Benjelloun, M., Schrijnemakers, K., Van Der Voort, P., Cool, P. & Vansant, E. F. (2002). *Chem. Mater.* **14**, 2317–2324.
Christenson, H. K. (2001). *J. Phys. Condens. Matter*, **13**, R95–R133.
Desplantier-Giscard, D., Galarneau, A., Di Renzo, F. & Fajula, F. (2003). *Mater. Sci. Eng. C*, **23**, 727–732.
Dolino, G., Bellet, D. & Faivre, C. (1996). *Phys. Rev. B*, **54**, 17919–17929.
Elsner, G., Riekel, C. & Zachmann, H. G. (1985). *Adv. Polym. Sci.* **67**, 1–57.
Evans, R. (1990). *J. Phys. Condens. Matter*, **2**, 8989–9007.
Gelb, L. D., Gubbins, K. E., Radhakrishnan, R. & Sliwinska-Bartkowiak, M. (1999). *Rep. Prog. Phys.* **62**, 1573–1659.
Gibson, L. J. & Ashby, M. F. (1999). *Cellular Solids, Structure and Properties*. Cambridge: Cambridge University Press.
Gusev, V. Y., Feng, X., Bu, Z., Haller, G. L. & O'Brian, J. A. (1996). *J. Phys. Chem.* **100**, 1985–1988.
Hammersley, A. P., Svensson, S. O., Hanfland, M., Fitch, A. N. & Häusermann, D. (1996). *High Press. Res.* **14**, 235–248.
Hartmann, M. & Bischof, C. (1999). *J. Phys. Chem. B*, **103**, 6230–6235.
Hartmann, M. & Vinu, A. (2002). *Langmuir*, **18**, 8010–8016.
Hofmann, T., Wallacher, D., Huber, P., Birringer, R., Knorr, K., Schreiber, A. & Findenegg, G. H. (2005). *Phys. Rev. B*, **72**, 064122.
Hoinkis, E. (2004). *Part. Part. Syst. Charact.* **21**, 80–100.
Kresge, C. T., Leonowicz, M. E., Roth, W. J., Vartuli, J. C. & Beck, J. S. (1992). *Nature*, **359**, 710–712.
Melnichenko, Y. B., Wignall, G. D., Cole, D. R. & Frielinghaus, H. (2006). *J. Chem. Phys.* **124**, 204711.
Mitropoulos, A. C., Haynes, J. M., Richardson, R. M. & Kanellopoulos N. K. (1995). *Phys. Rev. B*, **52**, 10035–10042.
Namatsu, H., Kurihara, K., Nagase, M., Iwadate, K. & Murase, K. (1995). *Appl. Phys. Lett.* **66**, 2655–2657.
Reichenauer, G. (2004). *Part. Part. Syst. Charact.* **21**, 117–127.
Reichenauer, G. & Scherer G. W. (2000). *J. Non-Cryst. Solids*, **277**, 162–172.
Scherer, G. W. (1992). *J. Non-Cryst. Solids*, **147–148**, 363–374.
Smarsly, B., Göltner, C., Antonietti, M., Ruland, W. & Hoinkis, E. (2001). *J. Phys. Chem. B*, **105**, 831–840.
Zhao, D., Feng, J., Huo, Q., Melosh, N., Fredrickson, G. H., Chmelka, B. F. & Stucky, G. D. (1998). *Science*, **279**, 548–552.
Zickler, G. A., Jähnert, S., Wagermaier, W., Funari, S. S., Findenegg, G. H. & Paris, O. (2006). *Phys. Rev. B*, **73**, 184109.